Finite-difference time-domain analysis of the tunneling and growing exponential in a pair of ε-negative and μ-negative slabs

Andrea Alù,[1,2,*] Nader Engheta,[1,†] and Richard W. Ziolkowski[3,‡]
[1]*University of Pennsylvania, Department of Electrical and Systems Engineering, Philadelphia, Pennsylvania 19104, USA*
[2]*University of Roma Tre, Department of Applied Electronics, Rome, Italy*
[3]*University of Arizona, Electrical and Computer Engineering Department, Tucson, Arizona 85721-0104, USA*
(Received 29 December 2005; published 18 July 2006)

Pairing together planar material slabs with opposite signs for the real parts of their constitutive parameters has been shown to lead in the steady-state regime to interesting and unconventional properties that are not otherwise observable for single slabs, such as resonance, anomalous tunneling, transparency, and subwavelength imaging through the reconstruction of evanescent waves [A. Alù and N. Engheta, IEEE Trans. Antennas Prop. **51**, 2558 (2003)]. The mechanics of the phenomenon, however, and in particular how the steady-state resonant response is reached, has not been explored. Here we analyze how a transient sinusoidal signal that starts at $t=0$ interacts with such a complementary pair of finite size using a finite-difference time-domain (FDTD) technique. Multiple reflections and transmissions at each interface are shown to build up to the eventual steady-state response of the pair, and during this process one can observe how the "growing exponential" phenomenon may actually occur inside this bilayer. As with any resonant phenomena, the time response of this effect depends on the Q of the system, which is related to the geometrical and electrical parameters of the bilayer. Transparency to finite beams and reconstruction of the subwavelength details of an image are shown in the transient and steady-state response of the setup through one-dimensional and two-dimensional FDTD simulations.

DOI: 10.1103/PhysRevE.74.016604 PACS number(s): 81.05.Zx, 41.20.Jb, 42.25.Bs, 03.50.De

I. INTRODUCTION

The current interest in understanding the physics behind the anomalous properties of metamaterials is evident in the recent physics and engineering literature. In particular, artificial materials with negative constitutive parameters, which can be distinguished into ε-negative (ENG), μ-negative (MNG) [1], and double-negative (DNG) [2] media if, respectively, their effective permittivity, permeability, or both of them have a negative real part, have been at the center of this attention, due to the anomalous phenomena theoretically predicted for their behavior and, in part, also verified experimentally. The existence and the possible artificial realization of these materials have been studied and verified. In particular, ENG (plasmonic) media exist naturally in the infrared and optical frequencies, e.g., noble metals below their plasma frequency [3] and polar dielectrics [4], and they can be relatively easily synthesized at lower frequencies by embedding a regular lattice of thin metallic wires in a host medium [5]. These inclusions provide the proper resonant electric polarizability in such an artificial material in the desired frequency regime. In analogy, an MNG material, such as a resonant ferromagnetic medium, may be synthesized by embedding resonant magnetic loops in a host medium, i.e., split-ring resonators, thereby providing the proper magnetic resonant polarizability in the desired frequency regime [6]. These two techniques may be employed at the same frequency to obtain DNG materials within a given frequency range, as has been reported in [7,8]. In practice, the current technology for manufacturing DNG materials consists of stacking together electrically thin layers of ENG and/or MNG materials, whose collections may be regarded as a bulk DNG medium [1]. To be consistent with the previous terminology, we will refer to common materials, which have both positive permittivity and permeability, as double-positive (DPS) materials.

One of the most striking properties of a planar DNG slab is represented by the possibility that it can focus subwavelength details, as first predicted in [9], by fostering the "growth" (instead of the decay) of evanescent waves inside it. Following this discovery, a multitude of papers explaining the potential implications and possible limitations of this anomalous phenomenon when realistic metamaterials are considered have appeared (see, e.g., Refs. [10–15]). Related to the aforementioned close analogy that exists between the DNG planar slab and a planar pair of ENG and MNG layers, it was demonstrated analytically in [1] that the "conjugate" (i.e., complementary) pairing of infinitely extent in two dimensions, juxtaposed planar slabs of ENG and MNG media (as well as DPS and DNG pairs, of which the *perfect* lens [9] is a special case), may induce an anomalous resonance, complete tunneling, total transparency, and reconstruction of evanescent waves, even though each of the two slabs by itself is essentially opaque to the incoming radiation.

The DNG "perfect lens" geometry has attracted a great deal of attention because of its striking consequences associated with the evanescent growth in such a simple geometry. Several studies have been devoted to analyzing the physics behind this anomalous phenomenon. In contrast, the physics and the mechanisms underlying the resonances of ENG-MNG pairs of complementary opaque materials have not re-

*Electronic address: alu@uniroma3.it
†Electronic address: engheta@ee.upenn.edu
‡Electronic address: ziolkowski@ece.arizona.edu

ceived as much attention and interest in the scientific community. These bilayers, however, are of strong interest for several reasons. First, ENG and MNG materials are relatively easier to manufacture separately than a bulk DNG material. Since only one of the two effective negative constitutive parameters must be realized in a given layer (not both), only one set of inclusions needs to be included to form that metamaterial layer. Second, the DNG itself may be regarded as a stack of such ENG and MNG pairs, if the bilayers are thin enough. Consequently, the physics involved with this pairing appears important also for a thorough understanding of DNG materials. Third, the same anomalous evanescent wave growth associated with a DNG slab is expected also in these bilayers. Finally, the resonances realized with such complementary pairs or with ENG or MNG materials paired with standard dielectrics have been proposed for several innovative devices, i.e., for guiding and radiating components of new conception (see, e.g., [16,17] and references therein). As for applications, it is worth emphasizing the possibility of a subwavelength imaging device achieved with an ENG-MNG bilayer as was suggested in [1], which is similar to the DNG perfect lens concept. This behavior is verified in the following sections.

It should be emphasized here that most of the studies on the physics associated with the anomalous properties of metamaterials, and in particular of DNG materials, have been performed analytically or numerically for the time-harmonic steady-state regime, i.e., under monochromatic excitation at a given fixed frequency, at which the involved metamaterials were supposed to have an ENG, MNG, or DNG response. However, the dispersive nature of these materials, which is well known to be necessary for energy conservation issues in passive materials with negative constitutive parameters [18], requires a certain time to establish this desired steady-state response [19]. Moreover, due to the resonant nature of the phenomena associated with these juxtaposed slabs and its connection to surface plasmons, it is clear that a certain amount of time is required to establish this behavior and it would be inversely related to the Q factor of this resonance. It is therefore expected that the response of these slab structures to a realistic initial excitation is not instantaneous, but would rely on some number of multiple reflections at each interface to establish the resonant mode.

In the following, we explore in detail the physical mechanisms underlying the anomalous resonance between an ENG and an MNG planar layer. In particular, we study how a transient sinusoidal signal would interact with such a juxtaposed ENG-MNG pair, showing how the multiple reflections and transmissions at each interface can be designed to build up to the eventual resonant steady-state response of the pair. We will demonstrate in detail that one can observe the "growing-exponential" phenomenon in this process as it occurs inside this bilayer. Here we have simulated this time-domain problem using the finite-difference time-domain (FDTD) technique, assuming the Drude models for the frequency dependence of the permittivity and permeability of these slabs. This choice allowed us to incorporate dispersive effects into the simulation model along with the possibility of having the material properties of both of these regions attain specified negative real parts at or approximately near

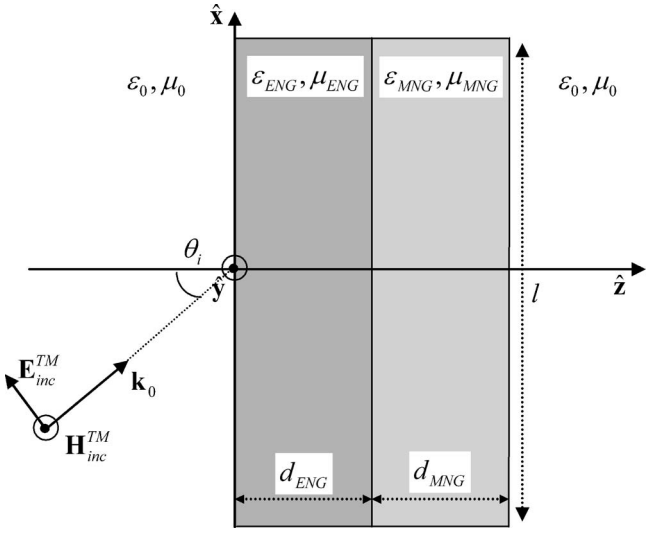

FIG. 1. A juxtaposed pair of planar finite sized slabs that are located in free space and are excited by a TM plane wave.

the frequency of the sinusoidal excitation. Our time-domain results confirm the steady-state prediction of growing exponential behavior in the bilayer and the total resonant transmission through it. However, as anticipated, these responses are achieved only after a certain period of time (i.e., a certain necessary number of FDTD time steps), which allows for the buildup of the interactions between the interfaces. Consequently, this time delay is found to be, in general, a function of the thickness of the slabs and the possible losses in each slab. A sketch of a small portion of these results was presented in a recent symposium [20].

II. FORMULATION OF THE PROBLEM

Two classes of numerical simulations were considered here: one dimensional (1D) and two dimensional (2D). The 1D problem represents a plane wave normally incident on a pair of infinitely extent ENG-MNG slabs. The two slabs have, respectively, the permittivity ε_{ENG}, ε_{MNG}, the permeability μ_{ENG}, μ_{MNG}, and the thicknesses d_{ENG}, d_{MNG} in the direction of propagation. In both the 1D and 2D simulations, the incident wave is turned on smoothly from a zero amplitude to a unit amplitude in five cycles.

The geometry of the 2D numerical problem is depicted in Fig. 1. Two planar slabs of transverse length l are surrounded by the empty space (with permittivity ε_0 and permeability μ_0) in a suitable Cartesian reference system. These two slabs also have, respectively, the permittivities ε_{ENG}, ε_{MNG}, the permeabilities μ_{ENG}, μ_{MNG}, and the thicknesses d_{ENG}, d_{MNG}. The excitation in the figure represents a TM (parallel polarized) plane wave impinging at a specified angle θ_i with respect to the normal. For simplicity, the geometry is independent of y. The actual excitation in the 2D simulations was a TM Gaussian beam; this provided us with the means to study the localization of the fields in the bilayer and beyond it.

When the materials have negative parameters, the constitutive parameters of the two materials composing the slabs under both the 1D and 2D analyses are assumed to follow the

lossy Drude models for their frequency dependence [2]. Their general form for a $e^{-i\omega t}$ time dependence may be written as

$$\varepsilon_{ENG}(\omega) = \varepsilon_0\left[1 - \frac{\omega_{peENG}^2}{\omega(\omega + i\Gamma_{eENG})}\right],$$

$$\mu_{ENG}(\omega) = \mu_0\left[1 - \frac{\omega_{pmENG}^2}{\omega(\omega + i\Gamma_{mENG})}\right]$$

$$\varepsilon_{MNG}(\omega) = \varepsilon_0\left[1 - \frac{\omega_{peMNG}^2}{\omega(\omega + i\Gamma_{eMNG})}\right], \quad (1)$$

$$\mu_{MNG}(\omega) = \mu_0\left[1 - \frac{\omega_{pmMNG}^2}{\omega(\omega + i\Gamma_{mMNG})}\right].$$

The electric and magnetic plasma frequencies ω_p may be chosen so that the two materials are, respectively, an ENG and an MNG medium at the driving radian frequency ω_d, at which the sinusoidal signal is launched. The Drude models represented by Eq. (1) satisfy the Kramers-Krönig and causality conditions, as widely discussed in the literature (see, e.g., [18]), and also the energy conservation requirements for passive ENG and MNG materials. Notice that these models include the presence of losses, represented by the collision frequency parameters Γ, and have a limited band of frequencies in which their constitutive parameters are negative, consistent with the limitations exhibited by real-life metamaterials. These models therefore represent valid choices for the following analyses. Note that when the considered materials have positive constitutive parameters with values not less than those of free space, their permittivity and permeability parameters are simply taken to be positive constants (i.e., dispersion is neglected in these cases).

In this context, we should underline that the current interest in materials and metamaterials with anomalous constitutive parameters has fostered also the interest of the scientific community in the numerical problems connected with regions of strong dispersion and absorption near the resonances of their constitutive parameters. In particular, FDTD modeling of metamaterials with strong dispersion has been presented in recent contributions (see, e.g., [21–23]), justifying the use of FDTD techniques in these regions. The results of the present paper, however, do not necessarily require excessively negative values of the permittivity or permeability to demonstrate these anomalous phenomena. The resonance considered here indeed concerns the pairing of materials with constitutive parameters of opposite signs. Therefore, we are not focused on materials having strong dispersive properties, and we can adequately demonstrate the effects with the simple Drude models (1), which satisfy causality and Kramers-Krönig relations [18]. We note also that for the negative permeability, Lorentzian or two-time-derivative Lorentzian dispersion models have also been used in the literature [6,7]. Here, however, for the sake of mathematical simplicity and faster convergence in the numerical simulations, the Drude model is used for both negative permittivity and permeability. This choice does not affect the general conclusions and nature of the results reported here.

As was shown analytically in [1] for infinite transverse width slabs, a $\sin(\omega_d t)$ monochromatic excitation of such a ENG-MNG pair structure would highlight its anomalous response at the frequency ω_d if the two media have *complementary* properties. Because the slabs under consideration here are finite in width, we expect similar behavior to occur from this bilayer when the same choice of the geometric and constitutive parameters is made, provided that the transverse dimension of the pair is large enough, i.e., $l \gg d_{ENG}, d_{MNG}$. With satisfaction of these conditions, we expect to achieve total tunneling of the radiation through the bilayer with little or no reflection, as well as the "growing" evanescent fields inside this pair and the subsequent possibility of virtual imaging with sub-wavelength resolution.

It is interesting to note that each of the two slabs per se would not allow propagation at the excitation frequency, since the wave number $k = \omega_d\sqrt{\mu\varepsilon}$ would be imaginary in either of them. Therefore, it is expected that the system would be highly reflective if one of the two slabs was removed. On the other hand, for the given TM plane wave impinging on the pair at the angle θ_i, the following conditions, which were derived in Ref. [1], Eq. (9), lead to the interface resonance:

$$\theta_i = \arcsin\sqrt{\frac{\varepsilon_{ENG}\varepsilon_{MNG}(\varepsilon_{MNG}\mu_{ENG} - \varepsilon_{ENG}\mu_{MNG})}{\mu_0\varepsilon_0(\varepsilon_{MNG}^2 - \varepsilon_{ENG}^2)}}, \quad (2)$$

$$\sqrt{\varepsilon_{ENG}\mu_{ENG}}d_{ENG} = \sqrt{\varepsilon_{MNG}\mu_{MNG}}d_{MNG},$$

These conditions ensure total tunneling, zero reflection and complete phase and amplitude restoration between the entrance and exit faces of the bilayer, in the limit of infinitely wide slabs ($l \to \infty$) and no losses. Similar expressions may be derived for the other polarization by invoking duality. An ENG-MNG pair illuminated by an incident plane wave that is designed following the resonance conditions in Eq. (2) will be denoted in the following discussion as a *conjugate pair* (or complementary pair), in analogy with Ref. [1].

As a special case, a *conjugate-matched* pair will denote the bilayers in which

$$\varepsilon_{ENG} = -\varepsilon_{MNG}, \quad \mu_{ENG} = -\mu_{MNG}, \quad d_{ENG} = d_{MNG}. \quad (3)$$

These conditions were shown in Ref. [1] to guarantee zero-reflection and total-transmission conditions for any TE or TM plane wave impinging on the pair, i.e., independent of the polarization and the angle of incidence. Moreover, when evanescent waves impinge on such conjugate-matched pairs, their incident amplitudes are restored as well on the back side of the bilayer. In [1] it was therefore further speculated that such conjugate-matched pairs may act as a virtual image displacer with subwavelength resolution, analogous in several ways to the perfect lens presented in [9].

III. TRANSIENT RESPONSE: FDTD SIMULATIONS

In this section we verify the analytical predictions reported in [1] and briefly discussed in the previous section

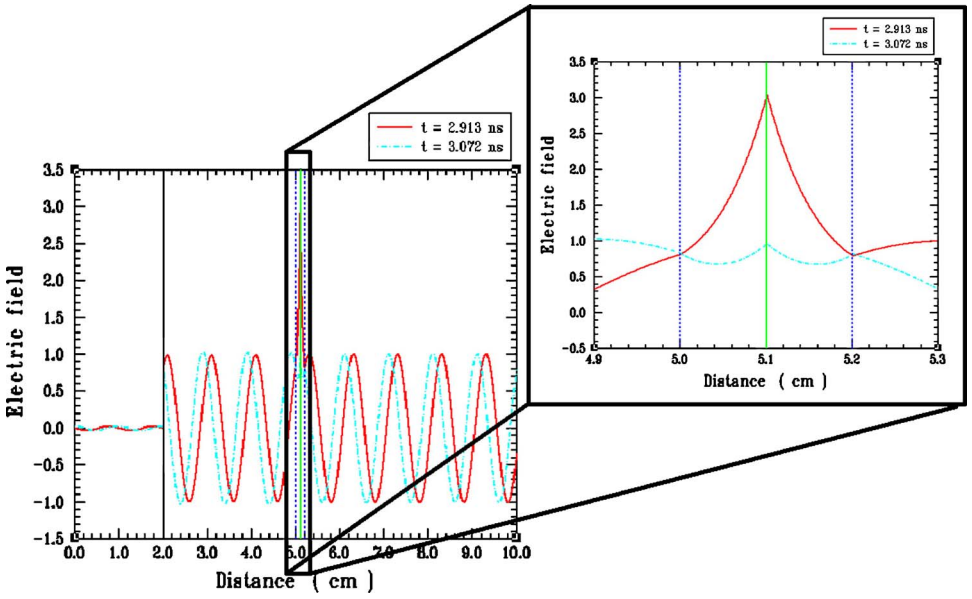

FIG. 2. (Color online) 1D FDTD simulation of a conjugate-matched pair at two different snapshots nearby in time in the steady-state regime [$\varepsilon_{ENG}(\omega_d) = -\varepsilon_{MNG}(\omega_d) = -3\varepsilon_0$, $\mu_{ENG}(\omega_d) = -\mu_{MNG}(\omega_d) = 2\mu_0$, $d_{ENG} = d_{MNG} = \lambda_0/10$, red line for $t = 2.913$ ns, blue line for $t = 3.072$ ns].

with selected numerical simulations generated with an FDTD engine (as in [2]). A sinusoidal excitation at the frequency ω_d that is smoothly turned on at $t=0$ is considered for both the 1D and 2D simulations. The spectrum of such an excitation is composed of an infinite number of harmonics centered on the frequency ω_d; this allows one to study the initial transient response of the system and its convergence towards the steady-state conditions.

A. 1D simulations

As a first example, we used the 1D simulator to study the behavior of a bilayer that was designed to be conjugate-matched pair at the frequency ω_d. The material parameters for this case were $\varepsilon_{ENG}(\omega_d) = -\varepsilon_{MNG}(\omega_d) = -3\varepsilon_0$, $\mu_{ENG}(\omega_d) = -\mu_{MNG}(\omega_d) = 2\mu_0$, $d_{ENG} = d_{MNG} = \lambda_0/10$, with $\lambda_0 = 2\pi/(\omega_d\sqrt{\varepsilon_0\mu_0}) = 1.0$ cm being the wavelength at the sinusoidal excitation frequency $f_0 = 30$ GHz. The problem space was 10 000 cells long, where $\Delta z = 10\ \mu\text{m} = \lambda_0/1000$. The source plane, a total field or scattered field boundary, was located at $z = 2000\Delta z$, the bilayer began at $z = 5000\Delta z$, $3\lambda_0$ away from the source. The thicknesses of the ENG and MNG layers were $d_1 = d_2 = 100\Delta z = \lambda_0/10$. The time step was $\Delta t = 0.95\Delta z/c = 31.67$ fs.

Figure 2 shows the electric field distribution inside and outside the bilayer, with a zoom for the distribution inside the conjugate-matched pair in the figure inset, at two different, but close snapshots in time when steady state has already been achieved. The plots clearly show the total tunneling predicted in [1], with the same phase at the entrance and the exit faces of the bilayer. Here and in the following figures the amplitude of the field is relative to the value of the incident wave in the steady-state regime, which was specified to be 1 V/m. It is evident at these time points that the growing-

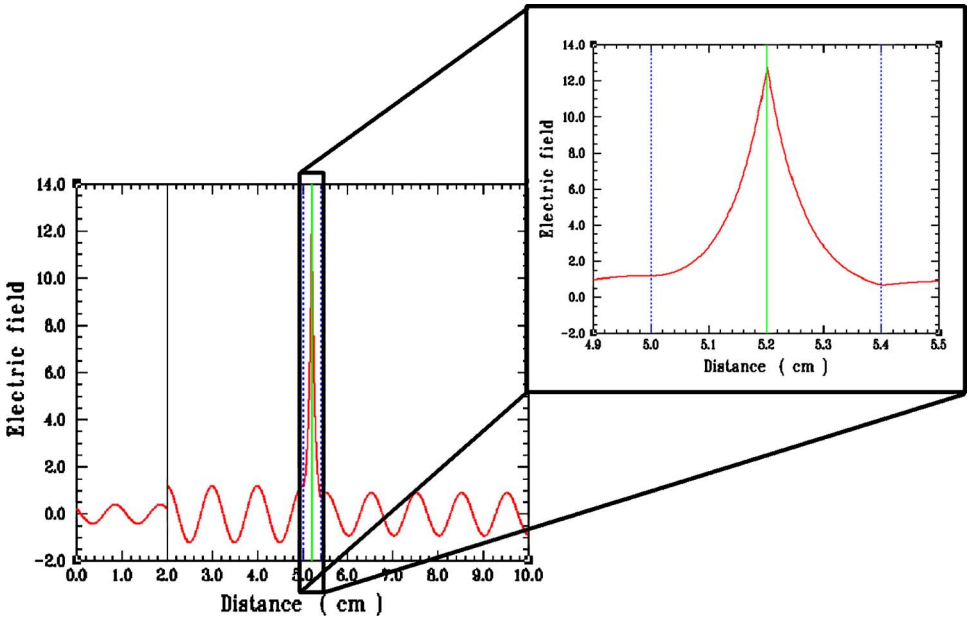

FIG. 3. (Color online) FDTD simulation of a conjugate-matched pair in the steady-state regime for $t = 9.476$ ns (the same as in Fig. 2, but with $d_{ENG} = d_{MNG} = \lambda_0/5$).

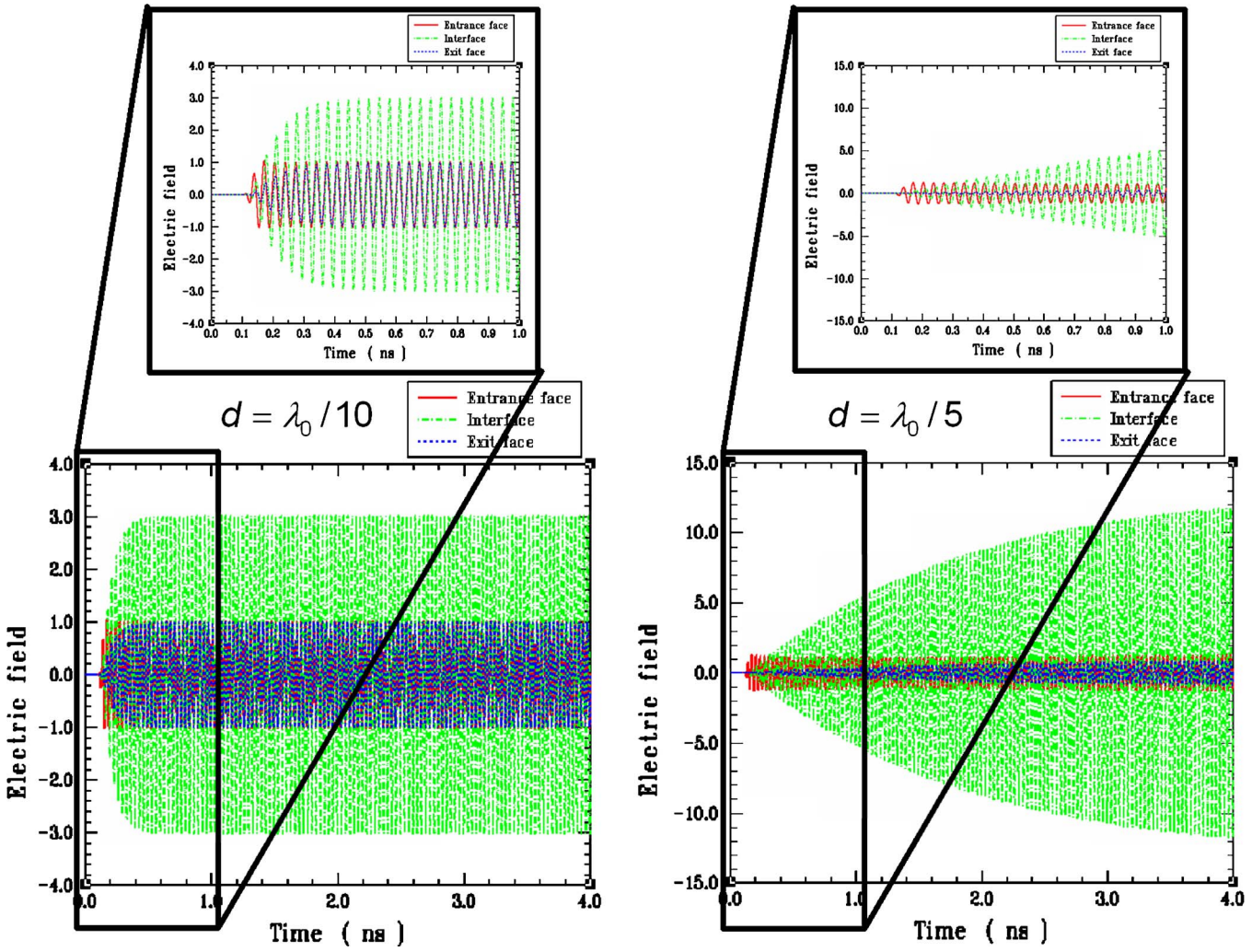

FIG. 4. (Color online) Time histories of the field values for the cases of Figs. 2 and 3 at the entrance and exit faces and at the interface (red line for the field at the entrance face, blue line at the exit face, and green line at the interface between the layers).

exponential distribution is already present, consistent with the fact that the wave is evanescent in each of the slabs of the bilayer, but its amplitude and phase is the same at the entrance and exit faces. Notice the sinusoidal variation in time of the exponential peak at the interface between the two layers, which is more evident in the zoom. As mentioned above, here and in the following plots some cells in the entrance side of the bilayer (here the first 2000 cells) are devoted to show only the reflected (scattered) field, isolated from the impinging excitation. As is evident, its amplitude is extremely low in this case, showing the total transmission typical of the steady-state regime for this conjugate-matched pair configuration.

Increasing the thicknesses of the layers to $d_{ENG}=d_{MNG}=\lambda_0/5$, one finds that it takes a longer period of time to reach the steady-state regime. A snapshot of the steady-state electric field at $t=9.476$ ns, a time comparable in the steady-state regime to those given in Fig. 2, is shown in Fig. 3. Again, the time elapsed from $t=0$ is long enough for the field inside the bilayer to experience the growing exponential, even though the level of reflection here is higher and the transmission amplitude is not complete.

Figure 4 shows the time history for the electric field values at the entrance (red line) and exit (blue line) faces and at the interface (green line) between the two media for the cases of Figs. 2 and 3. Here it is evident how the field at the entrance face rapidly converges to unity, whereas the interface field, which converges to a higher value due to the exponential growth predicted theoretically, requires a longer time to reach the steady state, consistent with the prediction that the multiple reflections inside the bilayer need some time to build up and achieve a final growing-exponential distribution inside the bilayer. This behavior is particularly apparent in the zoom of the first nanosecond in the two figures. It is also consistent with the fact that the spectrum of the excitation is converging towards ω_d, but in the transient the bilayer is not acting as a conjugate-matched pair, since its constitutive parameters have different responses at the different frequency components of the excitation. With a similar behavior, also the exit field converges slowly to unity, showing the total tunneling only after a transient period. Comparing the two cases of Fig. 4, it is clear how the steady-state regime is reached more slowly when thicker slabs are con-

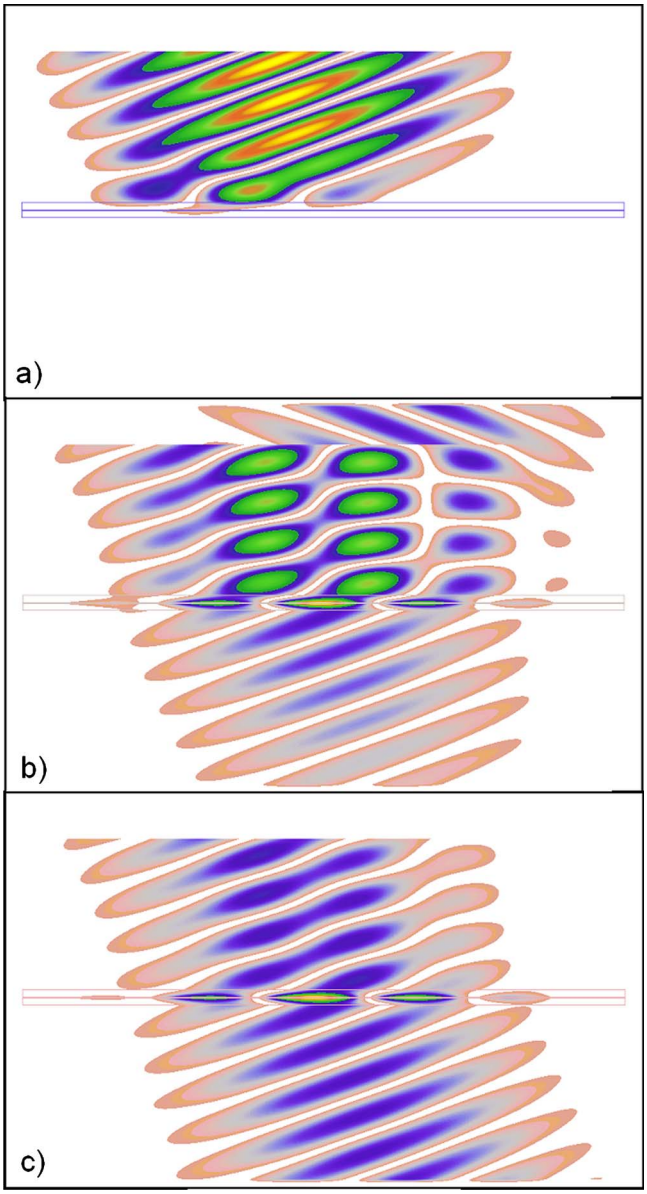

FIG. 5. (Color online) Three different snapshots in time (a) $t=600\Delta t=134.3$ ps, (b) $t=1200\Delta t=268.7$ ps, and (c) $t=3800\Delta t=850.8$ ps, for a Gaussian beam with $w_0=2\lambda_0$ incident at the angle $\theta_i=\pi/9=20°$ on the conjugate-matched pair of Fig. 2 (lighter colors correspond to higher values of the field).

sidered, since a larger thickness essentially corresponds to a higher resonance Q factor.

B. 2D simulations

The conclusions of the previous section have been further verified by considering the 2D case of a very broad Gaussian beam that was normally incident on a bilayer, each slab having the same depth as in the 1D examples. The distribution of the Gaussian beam in the total field-scattered field plane was $\exp(-x^2/w_0^2)$ where $w_0=5\lambda_0$. The time domain results were essentially the same. There was no noticeable impact on the rate of growth of the interface field of the finite transverse dimension of the slabs, and therefore these results are not reported here.

In Fig. 5 we show the results of a Gaussian beam with $w_0=2\lambda_0$ that is obliquely incident on the conjugate-matched bilayer having $d_1=d_2=\lambda_0/10$. The angle of incidence of the Gaussian beam was $\theta_i=\pi/9=20°$; the total transverse size of the slabs is $8\lambda_0$. The distribution of the electric field intensity is shown for three different instants in time. In the first snapshot, the beam has just arrived on the slab, and it starts its interaction with the bilayer. In the second snapshot, its interaction has started, but we are not yet in the steady-state regime. Here the fields start to build up at the interface between the slabs, while a visible, non-negligible reflected wave occurs and consequently creates an interference pattern with the incident wave. Entering the steady-state regime (third snapshot), however, the bilayer becomes totally transparent to the radiation, the fields are sensibly higher at the interface than in the outside region, and the reflection from the bilayer is zero. Notice also how the phase of the plane wave is totally restored at the exit face of the bilayer, as if the structure were completely transparent to the plane wave incidence.

The same behavior was also verified for a Gaussian beam with $w_0=0.5\lambda_0$ impinging with $\theta_i=\pi/9=20°$ on the same conjugate-matched bilayer. These results are shown in Fig. 6 in the left column. Since we are considering here, as in Fig. 5, a conjugate-matched bilayer, which in the steady state is transparent at every angle of incidence, we verify again in the last snapshot, given in Fig. 6(c), that total tunneling occurs through the bilayer even for this more complex and finite in space excitation. Again, note how the phase-restoration phenomenon is evident in the structure. In fact, one can see that the Gaussian beam actually tunnels in phase and amplitude through the bilayer when the steady state is reached.

We have also considered the conjugate bilayer case, which is designed following Eq. (2) to achieve the anomalous total tunneling only at the specific incidence angle $\theta_i=\pi/9=20°$, i.e., $\varepsilon_{ENG}(\omega_d)=-3\varepsilon_0$, $\mu_{ENG}(\omega_d)=2\mu_0$, $\varepsilon_{MNG}(\omega_d)=2\varepsilon_0$, $\mu_{MNG}(\omega_d)=-1.3\mu_0$, $d_{ENG}=d_{MNG}=\lambda_0/10$. The results are reported in the right column of Fig. 6, where it is evident how the total tunneling cannot be achieved in this case. Even in the steady-state regime, the impinging power is partially reflected back by the bilayer. Only a fraction of the plane waves that compose the Gaussian spectrum may tunnel through such a bilayer; and consequently a reflected wave remains present even after steady-state conditions are reached and a beam with a smaller angular spectrum tunnels through the bilayer even in the steady-state regime. The differences between the two cases are more evident in Fig. 7, where we compare the time responses that are generated when a Gaussian beam with a waist $w_0=\lambda_0$ impinges on the same two different bilayers used to generate Fig. 6. One can see that steady state is reached later in the conjugate-matched case than in the conjugate case, since more plane waves have to contribute to the resonance. Nonetheless, the tunneling is eventually complete (same amplitude and phase at the entrance and exit faces). In the conjugate case, on the other hand, steady state is reached more quickly, but the field at the exit face is lower than at the

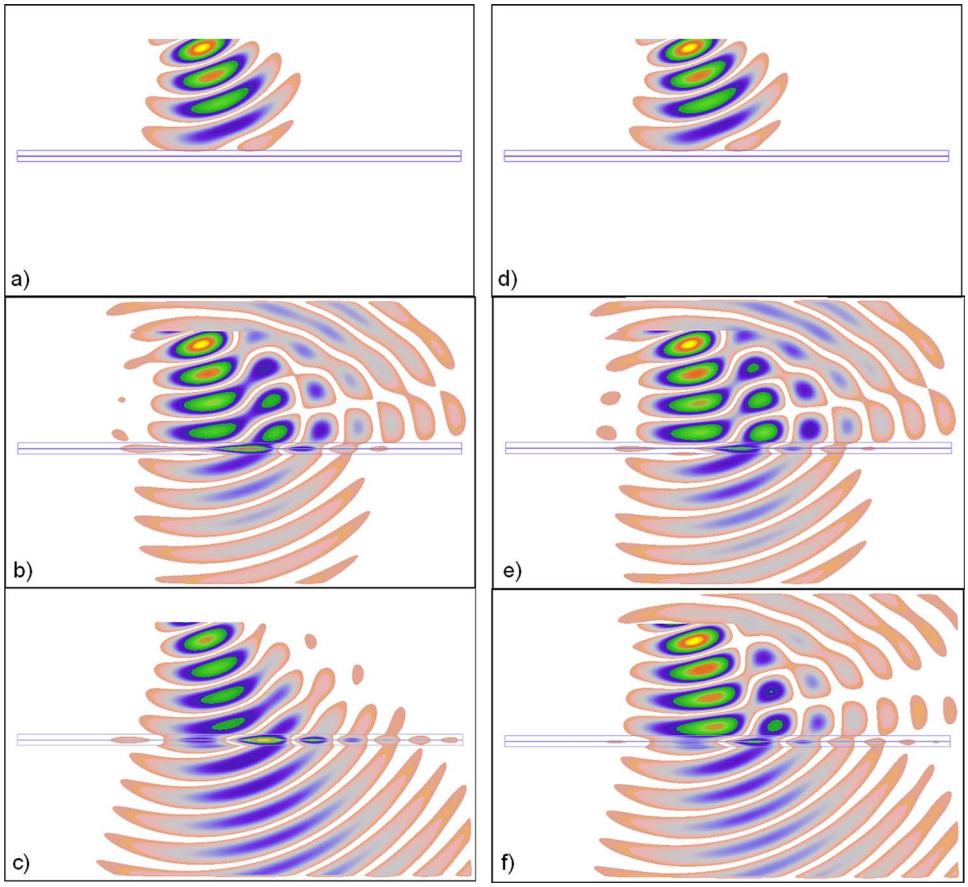

FIG. 6. (Color online) Three different snapshots in time (a) $t=600\Delta t=134.3$ ps, (b) $t=1200\Delta t=268.7$ ps, and (c) $t=3600\Delta t=806.0$ ps for a Gaussian beam with $w_0=0.5\lambda_0$ incident at the angle $\theta_i=\pi/9=20°$ on the conjugate-matched pair of Fig. 2; the same time snapshots in (d), (e), and (f) for the incidence on a conjugate pair with $\varepsilon_{ENG}(\omega_d)=-3\varepsilon_0$, $\mu_{ENG}(\omega_d)=2\mu_0$, $\varepsilon_{MNG}(\omega_d)=2\varepsilon_0$, $\mu_{MNG}(\omega_d)=-1.3\mu_0$, and $d_{ENG}=d_{MNG}=\lambda_0/10$ (lighter colors correspond to higher values of the field).

entrance. It is interesting to emphasize, moreover, how the fields at the interface get a higher value in the conjugate-matched case in comparison to the conjugate one. This is related again to the different numbers of plane waves that may actively contribute to the resonance. In other words, the conjugate-matched resonance indeed shows a higher Q factor, keeping fixed the thickness of the bilayer and the losses in the materials. [We remind the reader here that, as shown in [1], a given conjugate bilayer shows total tunneling at a single incident angle in the steady-state, represented by Eq. (2), but a sufficiently high transmission in a given angular region, whose broadness depends on the thickness of the bilayer and its other constitutive and geometrical parameters. This explains why the contribution from a superposition of plane waves to the resonance in the conjugate case is not represented by a single plane wave, but by a specific set of them.]

C. Virtual subwavelength imaging

In Fig. 8 we have tested the possibility of employing the bilayer as a virtual image displacer, as proposed in [1]. We have considered a line source on one side of the bilayer, a distance $d=20\Delta z=\lambda_0/5$ from it. It is clear from Fig. 8 that, after the time needed to reach a steady state, the phase and amplitude restoration at the exit side is complete, allowing

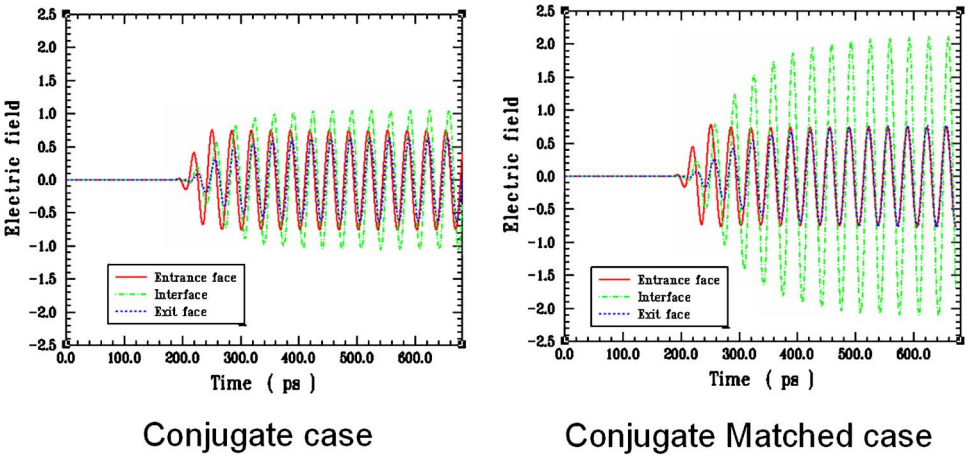

FIG. 7. (Color online) Time response for the same Gaussian beam ($w_0=\lambda_0$) impinging on a conjugate bilayer and on a conjugate-matched one (red line for the field at the entrance face, blue line at the exit face, and green line at the interface between the layers).

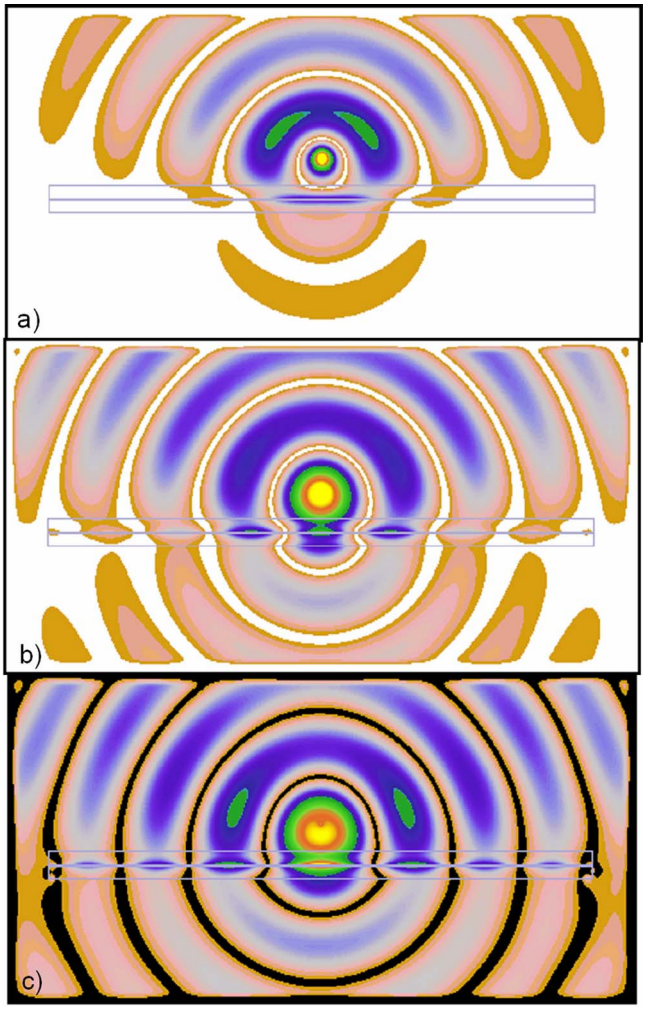

FIG. 8. (Color online) Three different snapshots in time (a) $t=600\Delta t=134.3$ ps, (b) $t=1000\Delta t=223.9$ ns, and (c) $t=1900\Delta t=425.4$ ps, for the employment of the conjugate-matched pair of Fig. 2 as a near-field virtual image displacer (lighter colors correspond to higher values of the field).

for an observer placed on the exit side of the bilayer to "view" the line current as if it were closer than it actually is. Also the reflection on the source side is minimal once steady state is reached.

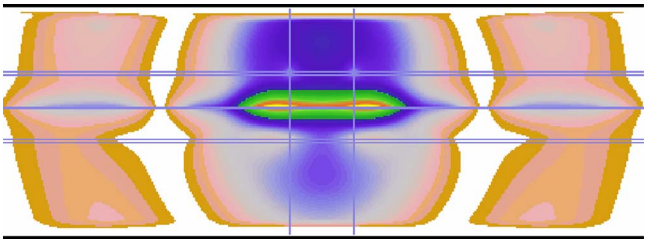

FIG. 9. (Color online) Snapshot in time for the electric field intensity at $t=4850\Delta t=1.715$ ns (in the steady-state regime) for two electric current line sources separated by $40\Delta z=\lambda_0/5$ located $0.01\lambda_0$ away from the bilayer of Fig. 8 (lighter colors correspond to higher values of the field).

As a final example, in Fig. 9 we have reported the steady-state regime electric field distribution for the same virtual displacer as in Fig. 8 when two sources with subwavelength spacing are placed close to the entrance side. The spacing between the sources is equal to $40\Delta z=\lambda_0/5$. You notice the expected large growth of the field at the ENG-MNG interface in the plot and how a blurry, but noticeable, resolution of the sources at the back face is clearly visible. In the figure, the vertical lines correspond to the position of the two sources and the horizontal lines delimit the ENG and MNG layers.

IV. CONCLUSIONS

In this contribution, using the FDTD technique we have analyzed thoroughly in the time domain the anomalous resonant phenomenon arising when pairing together material slabs with opposite signs for the real parts of their constitutive parameters. Complete tunneling, total transparency, reconstruction of evanescent waves, and subwavelength virtual imaging have been demonstrated numerically to occur after a reasonable time delay, even though each of the two slabs by itself would be essentially opaque to the incoming radiation. The effect works well even with transversally finite slabs and excitations, potentially leading to interesting applications for imaging tools. Physical insights and dependence of the time response to some of the parameters involved have been discussed.

[1] A. Alù and N. Engheta, IEEE Trans. Antennas Propag. **51**, 2558 (2003), special issue on metamaterials.
[2] R. W. Ziolkowski and E. Heyman, Phys. Rev. E **64**, 056625 (2001).
[3] P. B. Johnson and R. W. Christy, Phys. Rev. B **6**, 4370 (1972).
[4] M. Schall, H. Helm, and S. R. Keiding, Int. J. Infrared Millim. Waves **20**, 595 (1999).
[5] J. B. Pendry, A. J. Holden, D. J. Robbins, and W. J. Stewart, J. Phys.: Condens. Matter **10**, 4785 (1998).
[6] J. B. Pendry, A. J. Holden, D. J. Robbins, and W. J. Stewart, IEEE Trans. Microwave Theory Tech. **47**, 2075 (1999).
[7] R. A. Shelby, D. R. Smith, and S. Schultz, Science **292**, 77 (2001).
[8] D. R. Smith, W. J. Padilla, D. C. Vier, S. C. Nemat-Nasser, and S. Schultz, Phys. Rev. Lett. **84**, 4184 (2000).
[9] J. B. Pendry, Phys. Rev. Lett. **85**, 3966 (2000).
[10] S. A. Ramakrishna, J. B. Pendry, D. Schurig, D. R. Smith, and S. Schultz, J. Mod. Opt. **49**, 1747 (2002).
[11] J. T. Shen and P. M. Platzman, Appl. Phys. Lett. **80**, 3286 (2002).
[12] N. Garcia and M. Nieto-Vesperinas, Phys. Rev. Lett. **88**, 207403 (2002).

[13] M. W. Feise, P. J. Bevelacqua, and J. B. Schneider, Phys. Rev. B **66**, 035113 (2002).

[14] J. B. Pendry and S. A. Ramakrishna, Physica B **338**, 329 (2003).

[15] P. F. Loschialpo, D. L. Smith, D. W. Forester, F. J. Rachford, and J. Schelleng, Phys. Rev. E **67**, 025602 (2003).

[16] A. Alù and N. Engheta, in *Negative Refraction Metamaterials: Fundamental Properties and Applications*, edited by G. V. Eleftheriades and K. G. Balmain (John Wiley & Sons Inc., Hoboken, NJ, 2005), pp. 339–380.

[17] N. Engheta, A. Alù, R. W. Ziolkowski, A. Erentok, in *Metamaterials: Physics and Engineering Explorations*, edited by N. Engheta and R. Zioklowski (John Wiley and Sons, Inc., New York, 2006), pp. 43–86.

[18] L. Landau and E. M. Lifschitz, *Electrodynamics of Continuous Media* (Elsevier, New York, 1984).

[19] R. W. Ziolkowski and A. D. Kipple, Phys. Rev. E **68**, 026615 (2003).

[20] A. Alù, N. Engheta, and R. W. Ziolkowski, in Proceedings of USNC/CNC/URSI National Radio Science meeting, Monterey, CA, USA, June 20–26, 2004 (IEEE Press, New York, 2004), p. 18.

[21] J. Y. Lee, J. H. Lee, H. S. Kim, N. W. Kang, and H. K. Jung, IEEE Trans. Magn. **41**, 1484 (2005).

[22] M. W. Feise, J. B. Schneider, and P. J. Bevelacqua, IEEE Trans. Antennas Propag. **52**, 2955 (2004).

[23] L. Lu, Y. Hao, and C. G. Parini, IEE Proc.: Sci., Meas. Technol. **151**, 403 (2004).